Simplified continuum solvent model with a smooth cavity based on volumetric data

Alexander Held[1, a)] and Michael Walter[1, 2, b)]

[1)] *Freiburger Materialforschungszentrum, Albert-Ludwigs-Universität Freiburg, Stefan-Meier-Straße 21, D-79104 Freiburg, Germany*

[2)] *Fraunhofer IWM, Wöhlerstraße 11, D-79108 Freiburg, Germany*

We present a continuum solvent model (CSM) with a smooth cavity for the application in grid-based electronic structure methods. The cavity is identified with the inherently smooth distribution function of a binary mixture at infinite dilution. We obtain a cavity model based on atomic van der Waals radii and one free parameter controlling the overall size. This single parameter is sufficient to adequately reproduce experimental partial molar volumes. The CSM based on this cavity is of similar accuracy in the prediction of aqueous solvation Gibbs energies of small neutral molecules and ions as other CSMs with a smooth cavity. We apply the model to systems in non-aqueous solution, i.e. spiropyran/merocyanin energetics, a proton transfer reaction in dimethyl sulfoxide and the electrostatic screening of charged gold clusters in an ionic liquid.

PACS numbers: 31.70.Dk, 82.30.Qt, 82.30.Fi, 36.40.Wa

[a)] Electronic mail: Alexander.Held@fmf.uni-freiburg.de

[b)] Electronic mail: Michael.Walter@fmf.uni-freiburg.de

I. INTRODUCTION

Ab initio studies of molecules and surfaces are often treated in a vacuum at zero temperature due to the ease of description of such a fully defined situation. In reality, i.e. in experiment, this model does seldom correspond to the actual situation. Molecules, surfaces, and chemical reactions are most frequently studied in their solvated phase under ambient conditions.

The effects of the solvent on the solute under study can be manifold as the solvent molecules constantly scatter with themselves and the solute. The explicit inclusion of the solvent molecules into the ab initio description is mostly prohibitive due to the computational demand. In addition, a fully atomistic simulation at finite temperature requires the consideration of many different configurations that are effectively averaged by the dynamic environment. Indeed, there exist models that include the solvent molecules in a molecular mechanics description using classical force fields for example[1]. Such a detailed treatment of the solvent is often not needed, however.

One of the main effects on the solutes' electronic structure by the presence of the solvent is the effective screening of electric fields in its exterior in particular in the case of solvents of large polarizability. This effect can be efficiently described by a continuum averaging over the positions and orientations of the solvent molecules surrounding the solute[2]. These polarizable continuum models (PCMs) commonly assume a cavity inside the polarizable continuum that contains the solute. More generally, we will refer to models involving a continuum, possibly treating also non-polar interactions, as continuum solvent models (CSMs).

Traditionally, the homogeneous approximation[3] is applied for the definition of the cavity, meaning that the cavity is completely described by its boundary surface with vacuum inside and a homogeneous polarizable medium on the outside. This approach is implemented in many quantum chemistry codes[2] in the framework of Hartree-Fock, MP2, or coupled cluster methods and density functional theory (DFT) approaches. These implementations are traditionally based on atom-localized basis sets. The electrostatic interaction can then be calculated by solving the vacuum Poisson equation with special boundary conditions at the cavity surface[2], for example by placing screening charges at the cavity boundary[4].

There are efficient DFT implementations that are based on grids either in momentum (plane waves) or configuration space. These have problems with the homogeneous approximation, that includes discontinuities in the dielectric permittivity $\epsilon(\boldsymbol{r})$ at the cavity surface which are only poorly representable in grid bases. In their pioneering work, Fattebert and Gygi[5] presented a formulation of a PCM that works well together with grid-based implementations. The authors used a smooth permittivity function $\epsilon(\boldsymbol{r})$ in the Poisson equation

$$\nabla\left(\epsilon(\boldsymbol{r})\nabla\Phi(\boldsymbol{r})\right) = -4\pi\rho(\boldsymbol{r}) \tag{1}$$

to obtain the electrostatic potential $\Phi(\boldsymbol{r})$ of the total solute charge distribution $\rho(\boldsymbol{r})$ within the polarizable medium. The permittivity $\epsilon(\boldsymbol{r})$ is then represented on the same grids as the solute electron density. It is taken to be unity in the region of the solute and agrees with the dielectric constant of the solvent at far distance from the solute. The transition between these regions is modeled as a smooth function depending on the electron density. Such a smoothly defined cavity also allows to calculate accurate forces acting on the solute nuclei, applicable to structure optimization or molecular dynamics in solution[6].

It turned out, that the self-consistent definition of the smooth cavity as a function of the electron density can lead to numerical instabilities. Sánchez *et al.*[7] presented an implementation that is capable of treating solid surface interfaces in the presence of a polarizable solvent[7] based on their earlier approach[8], but with improved numerical stability by defining the cavity in a non-self-consistent way from the positions of the nuclei and tabulated van der Waals radii.

Recently Andreussi *et al.*[9] presented a revised version of the original model from Fattebert and Gygi, where the authors attacked the numerical instabilities by choosing the form of the smooth step function according to numerical considerations. Dziedzic *et al.*[10] determined the cavity once from the pre-calculated electron density in the gas phase in order to overcome the numerical instabilities. These authors also pointed out, that the self-consistent variation of the cavity with the electron density yields unphysical behavior for charged systems in water for a fixed set of parameters.

In the present work, we contribute to the field of smooth cavity CSMs by a different approach to the parametrization. We follow the idea of creating a smooth cavity from atomic positions and van der Waals radii as presented by Sánchez *et al.*[7], but replace the smooth step function introduced by Fattebert and Gygi[5] by a physically motivated one. Instead of obtaining the optimal description for the cavity by fitting to solvation free energies, we determine the form of the cavity from independent experimental volumetric data. The cavity created by the solute in the solvent is identified as an effective solute-solvent pair distribution function of a non-self-interacting solvent as described in the following section.

Section III lays out the general framework for CSMs with a smooth cavity and Section V covers implementational details, notably the peculiarities of the projector augmented waves[11,12] (PAW) formalism and the performance of the Poisson solver. The parametrization of the model is illustrated in Sections VI and VII along with test cases involving neutral molecules, cations and anions. The application of the model to different systems in non-aqueous solution is finally presented in Section VIII.

II. THE SOLUTES' CAVITY

The first problem arising in any CSM is the question how to define the cavity that is produced by the solute when it is present in the continuum representing the solvent[2]. Considering only spatial degrees of freedom for the solvent molecules as a whole, the cavity can generally be described by the mass or number density $\rho_L(\boldsymbol{r})$ of the solvent. Equivalently the distribution function $g(\boldsymbol{r}) = \rho_L(\boldsymbol{r})/\rho_0$ with ρ_0 the density of the pure solvent[3] can be used, where $\boldsymbol{r}$ is a spatial coordinate with respect to the solute in a fixed configuration.

The above mentioned homogeneous approximation divides space into a region excluding the solvent completely, and a region where the solvent is present as in its liquid bulk phase. The corresponding distribution function describing the cavity C is then

$$g(\boldsymbol{r}) = \begin{cases} 0 & \text{if } \boldsymbol{r} \in C \\ 1 & \text{if } \boldsymbol{r} \notin C \end{cases}, \tag{2}$$

where it is sufficient to define the cavity's boundary ∂C, for example by interlocked spheres.

An alternative to the hard wall cavity is a smoothly defined distribution function. The smoothness can be interpreted as a result of the dynamic nature of the solvent-solute interaction, in that it is connected to the probability of their approach. In addition a smooth distribution function is more appropriate for grid-based calculations and facilitates the numerical treatment of the forces on the solute nuclei[6].

Applying the statistical mechanical model of Kirkwood and Buff[13], the distribution function $g(\boldsymbol{r})$ of the solvent around the solute is found to be the distribution function $g(\boldsymbol{r}) = g_{LM}(\boldsymbol{r})$ between the constituents of an infinitely dilute binary mixture, where the index L stands for solvent and M for the solute molecule. The function $g_{LM}(\boldsymbol{r})$ typically has a complex structure showing a peak in the first solvation shell and oscillatory behavior for the outer solvation shells as sketched in Figure 1. It is related to the partial molar volume (per molecule) $\overline{v}_M^\infty$ of the solute through the compressibility equation in the limit of infinite dilution[13,14]

$$\int \big(1 - g_{LM}(\boldsymbol{r})\big)\mathrm{d}\boldsymbol{r} = \overline{v}_M^\infty - \kappa_T k_\mathrm{B} T, \tag{3}$$

with the isothermal compressibility of the solvent κ_T. The partial molar volume is an experimentally accessible quantity[15–20] and the term $\kappa_T k_\mathrm{B} T$ is typically small as compared to $\overline{v}_M^\infty$.

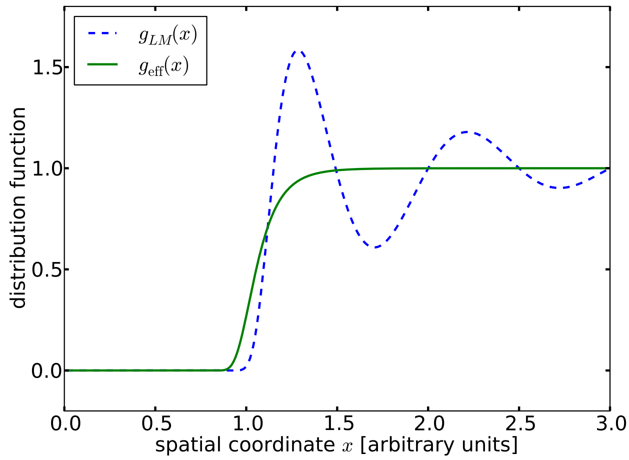

Figure 1. Sketch of a typical solvent-solute distribution function $g_{LM}(x)$ and an effective distribution function $g_{\mathrm{eff}}(x)$ fulfilling eq. (6).

In order to carry out an approximation for the distribution function $g_{LM}(\boldsymbol{r})$, we employ the equivalent formulation using a mean potential $u_{LM}(\boldsymbol{r})$ via the Boltzmann distribution[21]

$$g_{LM}(\boldsymbol{r}) = \exp\left(-\frac{u_{LM}(\boldsymbol{r})}{k_\mathrm{B}T}\right) \tag{4}$$

such that $u_{LM}(\boldsymbol{r})$ is the average work necessary to bring a solvent molecule from infinite separation from the fixed solute molecule to position $\boldsymbol{r}$. The averaging has to be carried out over all solvent degrees of freedom except the position $\boldsymbol{r}$ of a single solvent molecule for a given thermodynamic ensemble of the solvent molecules. For a (hypothetical) non-self-interacting solvent, the mean potential $u_{LM}(\boldsymbol{r})$ coincides with the solvent-solute potential. In general, the mean potential can be interpreted as the effective solvent-solute potential $u_{\mathrm{eff}}(\boldsymbol{r})$

of a non-self-interacting solvent reproducing the same solvent-solute distribution function as the original self-interacting solvent. We employ such an effective, non-self-interacting solvent with an effective solvent-solute potential $u_{\text{eff}}(\boldsymbol{r})$ and a distribution function

$$g_{\text{eff}}(\boldsymbol{r}) = \exp\left(-\frac{u_{\text{eff}}(\boldsymbol{r})}{k_{\text{B}}T}\right). \tag{5}$$

Yet we loosen the condition $g_{\text{eff}} = g_{LM}$ of reproducing the distribution function exactly to only reproducing the volume integral from the compressibility equation (3)

$$\begin{aligned} \int \big(1 - g_{\text{eff}}(\boldsymbol{r})\big)\mathrm{d}\boldsymbol{r} &= \int \big(1 - g_{LM}(\boldsymbol{r})\big)\mathrm{d}\boldsymbol{r} \\ &= \overline{v}_M^{\infty} - \kappa_T k_{\text{B}}T \end{aligned}. \tag{6}$$

This condition can be validated without the knowledge of the true distribution function g_{LM} by performing a simple volume integral for a given solute geometry and comparing the result to experimental data. The complexity of the problem is reduced as we now have the freedom to employ an approximation for the effective potential. In particular, we choose $u_{\text{eff}}(\boldsymbol{r})$ to be repulsive only and build it from the positions of the nuclei and van der Waals radii. The requirement of a purely repulsive effective potential produces a monotonic transition from 0 near the solute to 1 far from the solute for $g_{\text{eff}}(\boldsymbol{r})$ as sketched in Figure 1 and benefits to numerical stability[9].

Since we have the single condition eq. (6), we are looking for a repulsive potential with a single free parameter that controls the size of the cavity. Motivated by the repulsive term in the Lennard-Jones potential and its simplicity, we assume an effective repulsive potential of the form

$$u_{\text{eff}}(\boldsymbol{r}) = u_0 \sum_a \left(\frac{R_a^{\text{vdW}}}{\|\boldsymbol{r} - \boldsymbol{R}_a\|}\right)^{12} \tag{7}$$

between the solute molecule fixed in the simulation cell and a solvent particle at position $\boldsymbol{r}$. The summation runs over all atoms a of the solute molecule with van der Waals radii $\{R_a^{\text{vdW}}\}$ and positions $\{\boldsymbol{R}_a\}$ of the nuclei. We remind, that this effective repulsive potential is not to be confused with the repulsive part of the true solute-solvent interaction[22–24], but contains the attractive solvent-solute and the solvent-solvent interactions implicitly.

Once a set of van der Waals radii has been chosen, the only free parameter is the value u_0 of the potential at the van der Waals radius, which can be fitted to experimental volumes $\overline{v}_M^{\infty} - \kappa_T k_{\text{B}}T$ using eqs. (5) and (6). A similar model was sketched by Im *et al.*[6] for the use in molecular mechanics calculations. There, the smooth distribution function was introduced for numerical reasons only, without explicitly specifying the potential or relating the distribution function to experimental volumetric data, however.

We will show below for the example of water, that this simple approach not only leads to a good description of measured partial volumes for the molecular test set used for fitting, but is also able to predict the partial volumes of other molecules within the solvent.

III. CONTINUUM SOLVENT MODELS WITH A SMOOTH CAVITY

Before going further to describe how we model the interactions between solute and solvent, we discuss the general framework of CSMs with a smooth cavity. The models currently available in the literature[5,7–10], including the model presented in this work, can technically all be described as consisting of the following parts:

- a cavity/distribution function $g(\boldsymbol{r}, n, \{\boldsymbol{R}_a\})$ as defined above,
- a dielectric permittivity function $\epsilon(g)$,
- a Poisson solver for eq. (1) and
- a set of additional solvent-solvent or non-polar solvent-solute interactions summing up to an interaction free energy $G_{\text{ia}}[g, n, \{\boldsymbol{R}_a\}]$,

where n denotes the solute electron density and $\{\boldsymbol{R}_a\}$ the atomic positions. This composition reflects the splitting of the solvation Gibbs energy[25] usually applied in quantum mechanical CSMs[2]

$$\Delta G_{\text{S}}^{*} = \Delta G_{\text{el}} + G_{\text{cav}} + G_{\text{rep}} + G_{\text{dis}} + \Delta G_{\text{tm}} \ . \tag{8}$$

The term ΔG_{el} describes a change in energy due to the electrostatic solvent-solute and solute-self-interaction as compared to a gas phase calculation. The term G_{cav} is the cavity formation energy, i.e. the energy needed to create the cavity. G_{rep} and G_{dis} stand for the repulsion and dispersion contributions to the solvent-solute interaction, which we refer to as non-polar interactions. The term ΔG_{tm} finally denotes the change in free energy arising from the difference in the rotational and vibrational thermal motion in the gas phase and in solution.

In order to see, how the constituents of a CSM with a smooth cavity relate to the decomposition in eq. (8), we start from the total energy in the Kohn-Sham formulation of DFT[26] which can be written as

$$E_0[n, \{\boldsymbol{R}_a\}] = E_{\mathrm{kin}}[n] + E_{\mathrm{xc}}[n] + E_{\mathrm{C}}[n, \{\boldsymbol{R}_a\}], \tag{9}$$

with the kinetic energy of the system of non-interacting electrons E_{kin} and the exchange-correlation energy E_{xc}. The Coulomb energy is expressed as

$$E_{\mathrm{C}}[n, \{\boldsymbol{R}_a\}] = \frac{1}{2} \int \rho(\boldsymbol{r}) \Phi(\boldsymbol{r}) \mathrm{d}\boldsymbol{r}\, , \tag{10}$$

and contains all electrostatic contributions as ρ includes both the electron density n, as well as the charges of the nuclei. The corresponding Φ is the solution of the vacuum Poisson equation

$$\Delta \Phi(\boldsymbol{r}) = -4\pi \rho(\boldsymbol{r})\, , \tag{11}$$

where the self-interaction of the nuclear point charges has to be excluded in eq. (10).

The electrostatic interaction in solution is modified by the dielectric permittivity function $\epsilon(g)$. The expressions (9) and (10) are still valid when the vacuum Poisson equation (11) is replaced by the Poisson equation (1) including ϵ. We assume, that the additional non-polar interactions and the cavity formation energy can be written as a volume integral over a function f_{ia} depending semi-locally on the cavity, the electron density[27] and the atomic positions. Together, these terms yield the additional interaction that can be expressed as

$$\begin{aligned} G_{\mathrm{ia}} &= G_{\mathrm{cav}} + G_{\mathrm{rep}} + G_{\mathrm{dis}} \\ &= \int f_{\mathrm{ia}} \Big(\{\nabla^i g_{\mathrm{eff}}(\boldsymbol{r})\}, \{\nabla^i n(\boldsymbol{r})\}, \{\boldsymbol{R}_a\} \Big) \mathrm{d}\boldsymbol{r}\, . \end{aligned} \tag{12}$$

In conclusion, the free energy in solution can be written as

$$\begin{aligned} G[n, \{\boldsymbol{R}_a\}] =& E_{\mathrm{kin}}[n] + E_{\mathrm{xc}}[n] + E_{\mathrm{C}}[\epsilon(g), n, \{\boldsymbol{R}_a\}] \\ & + G_{\mathrm{ia}}[g, n, \{\boldsymbol{R}_a\}] \end{aligned} \tag{13}$$

where the electron density n is generally not the same as in vacuum. The kinetic energy functional for the non-interacting system remains unchanged and we assume the same to be true for the exchange-correlation term[28].

The solvation Gibbs energy is obtained as

$$\Delta G^*_{\mathrm{S}} = G[n, \{\boldsymbol{R}_a\}] - E_0[n_0, \{\boldsymbol{R}_a\}] + \Delta G_{\mathrm{tm}} \tag{14}$$

where n_0 and n are the ground state solute electron densities in the gas phase and in solution, respectively. The explicit expression for the electrostatic term is

$$\begin{aligned}\Delta G_{\mathrm{el}} =& E_{\mathrm{kin}}[n] - E_{\mathrm{kin}}[n_0] \\ &+ E_{\mathrm{xc}}[n] - E_{\mathrm{xc}}[n_0] \\ &+ E_{\mathrm{C}}[\epsilon(g), n, \{\boldsymbol{R}_a\}] - E_{\mathrm{C}}[\epsilon = 1, n_0, \{\boldsymbol{R}_a\}]\,.\end{aligned} \tag{15}$$

Notably ΔG_{el} also includes changes to the kinetic and exchange-correlation terms due to the altered ground state electron density in solution and G_{ia} may also affect the ground state if it depends on the electron density (either explicitly or implicitly through the cavity) in a particular model. In the above description, we have assumed the same geometry $\{\boldsymbol{R}_a\}$ in the gas phase and in solution. Structural changes can be accounted for by optimizing the geometry in solution which is vastly accelerated if the forces on the nuclei are known. We describe below, what is necessary for finding the ground state electron density and the forces in solution.

The calculation of the effective single-particle wave functions involves the Kohn-Sham potential, that is given by[26]

$$v_{\mathrm{KS}} = \frac{\delta(E - E_{\mathrm{kin}})}{\delta n} \tag{16}$$

and we will now discuss the different contributions separately. The Coulomb energy E_{C} introduces a term $v_{\mathrm{C}} = \frac{\delta E_{\mathrm{C}}}{\delta n}$ to the Kohn-Sham potential. In a gas phase calculation, v_{C} is simply the electrostatic potential Φ[26]. In the presence of a dielectric, there is an additional term[5]

$$v_{\epsilon} = -\frac{1}{8\pi}\frac{\partial \epsilon}{\partial g}\frac{\partial g}{\partial n}\left\|\nabla\Phi\right\|^2 \tag{17}$$

that is only nonzero if the cavity depends on the electron density. This term has been identified as a source of numerical instabilities[10] and is therefore mostly avoided. The term $\frac{\delta E_{\mathrm{xc}}}{\delta n}$ arising from the exchange-correlation term is analog to a gas phase calculation. The additional interaction G_{ia} introduces

$$v_{\mathrm{ia}} = \frac{\delta G_{\mathrm{ia}}}{\delta n} = \frac{\eth G_{\mathrm{ia}}}{\eth g}\frac{\partial g}{\partial n} + \frac{\eth G_{\mathrm{ia}}}{\eth n} \tag{18}$$

to the Kohn-Sham potential, where $\eth$ denotes the partial functional derivative. Altogether, the Kohn-Sham potential in solution is thus

$$v_{\mathrm{KS}} = \frac{\delta E_{\mathrm{xc}}}{\delta n} + \Phi + v_{\epsilon} + v_{\mathrm{ia}}\,. \tag{19}$$

Due to the presence of the dielectric and the additional interaction, also the expression of the forces on the nuclei is modified. Let $\partial_{a\nu} = \frac{\partial}{\partial(\boldsymbol{R}_a)_\nu}$ be the partial derivative for the ν^{th} component of the position of atom a. The ν^{th} component of the force on nucleus a due to the explicit dependence of the Coulomb energy E_C on the atomic positions can be written as[7]

$$-\partial_{a\nu} E_\text{C} = -\int \Phi \partial_{a\nu} \rho \, \mathrm{d}\boldsymbol{r} + (F_\text{C})_{a\nu} \tag{20}$$

where the first term on the right hand side is analog to a gas phase calculation and the additional contribution is

$$(F_\text{C})_{a\nu} = \frac{1}{8\pi} \int \frac{\partial \epsilon}{\partial g} (\partial_{a\nu} g) \left\| \nabla \Phi \right\|^2 \mathrm{d}\boldsymbol{r} \; . \tag{21}$$

Additionally, the interaction G_ia gives rise to a force contribution

$$(F_\text{ia})_{a\nu} = -\int \left(\frac{\eth G_\text{ia}}{\eth g} \partial_{a\nu} g + \partial_{a\nu} f_\text{ia} \right) \mathrm{d}\boldsymbol{r} \; . \tag{22}$$

In conclusion, a specific CSM with a smooth cavity involves the following derivatives for obtaining the Kohn-Sham potential and the forces in solution:

$$\frac{\partial g}{\partial n}, \quad \partial_{a\nu} g, \quad \frac{\partial \epsilon}{\partial g}, \quad \frac{\eth G_\text{ia}}{\eth g}, \quad \frac{\eth G_\text{ia}}{\eth n}, \quad \partial_{a\nu} f_\text{ia} \tag{23}$$

Now we are prepared to present the remaining part of our specific CSM with a smooth cavity in the following section.

IV. THE DIELECTRIC AND SURFACE TERMS

Having defined the cavity in sec. II, we are able to switch on the electrostatic interaction between the solute molecule and the solvent. As motivated in Ref. 6, we take the electric susceptibility to be directly proportional to the effective distribution function $g_\text{eff}(\boldsymbol{r})$ such that the electrostatic screening is modeled as a position dependent dielectric function (i.e. relative permittivity)

$$\epsilon(g_\text{eff}(\boldsymbol{r})) = 1 + (\epsilon_\infty - 1) g_\text{eff}(\boldsymbol{r}) \tag{24}$$

where ϵ_∞ is the experimentally determined macroscopic dielectric constant of the pure solvent. Eq. (24) is the analog of eq. (64) in the work of Andreussi *et al.*[9] and eqs. (7) and (12) in the work of Scherlis *et al.*[8] with the identification $g_\text{eff}(\boldsymbol{r}) = 1 - \vartheta(\boldsymbol{r})$. The difference in mentality is, that our starting point is not the smooth dielectric function $\epsilon(\boldsymbol{r})$ fitted to experimental solvation Gibbs energies or results from previous solvation models with the cavity $\vartheta(\boldsymbol{r})$ as a derived quantity. Instead, in our approach, $\epsilon(\boldsymbol{r})$ emanates from the definition of the cavity fitted to independently determined experimental partial molar volumes.

The remaining question is how to describe the non-electrostatic terms. We treat them together as a geometric term ΔG_{geo} and assume that their sum is proportional to the cavity surface area A

$$\Delta G_{\mathrm{geo}} = G_{\mathrm{cav}} + G_{\mathrm{rep}} + G_{\mathrm{dis}} + \Delta G_{\mathrm{tm}} = \gamma A\,. \tag{25}$$

For the cavity formation energy and the dispersion and repulsion contribution, this is a widely used and reasonable approximation[6,9,10]. We have also included ΔG_{tm} into eq. (25) as we will fit the proportionality factor γ to experimental solvation Gibbs energies containing this contribution. Having defined the forces, this term could be explicitly calculated, which we avoid for the ease of computation.

In contrast to the homogeneous approximation, the cavity surface corresponding to a smooth cavity $g(\boldsymbol{r})$ is not well defined. Assuming a monotonic transition, a simple choice could be the isosurface at a fixed value of $g(\boldsymbol{r})$ and there are several techniques available for the extraction of isosurfaces from volumetric data[29,30]. We follow the elegant approach suggested in Ref. 6, where g in the full configuration space is used and the cavity surface area is defined as

$$A[g] = \int \|\nabla g(\boldsymbol{r})\|\,\mathrm{d}\boldsymbol{r}\,. \tag{26}$$

For a discontinuous step function $g(\boldsymbol{r})$ as in the homogeneous approximation, $\|\nabla g(\boldsymbol{r})\|$ is peaked at the well defined cavity surface and the according area is reproduced exactly. We show in Appendix A, that eq. (26) is the limit $\Delta \to 0$ of the definition of the cavity surface area used in the work of Andreussi *et al.*[9] (eq. (63)) that depends on a finite difference parameter Δ. We note that, depending on the particular shape of g, $A[g]$ is not necessarily the area of the isosurface $g(\boldsymbol{r}) = \frac{1}{2}$. In our case, for an effective cavity $g_{\mathrm{eff}}(\boldsymbol{r})$ constructed from a single atom, $A[g_{\mathrm{eff}}]$ is the area of the isosurface $g_{\mathrm{eff}}(\boldsymbol{r}) = \exp\left(-\Gamma(\frac{5}{6})^{-6}\right) \approx 0.62$ as shown in Appendix A.

As described in Section III, the self-consistent procedure for finding the ground state electron density in Kohn-Sham DFT and the calculation of the forces require certain derivatives of the cavity, the dielectric function and the additional interaction term. The effective cavity

$g_{\text{eff}}(\boldsymbol{r})$ does not depend on the solute electron density in our model. We have an additional interaction term proportional to the cavity surface area (c.f. eq. (12))

$$G_{\text{ia}}[g_{\text{eff}}] = \gamma A[g_{\text{eff}}] = \int f_{\text{ia}}\Big(\nabla g_{\text{eff}}(\boldsymbol{r})\Big)\mathrm{d}\boldsymbol{r} \tag{27}$$

with

$$f_{\text{ia}}\Big(\nabla g_{\text{eff}}(\boldsymbol{r})\Big) = \gamma \left\|\nabla g_{\text{eff}}(\boldsymbol{r})\right\| \tag{28}$$

that does neither explicitly depend on the solute electron density nor on the atomic positions.

In conclusion, the derivatives in our model read

$$\begin{aligned} \frac{\partial g_{\text{eff}}}{\partial n} &= 0, & \frac{\eth G_{\text{ia}}}{\eth n} &= \partial_{a\nu} f_{\text{ia}} = 0, \\ \frac{\partial \epsilon}{\partial g_{\text{eff}}} &= \epsilon_\infty - 1, & \frac{\eth G_{\text{ia}}}{\eth g_{\text{eff}}} &= -\gamma \operatorname{div}\left(\frac{\nabla g_{\text{eff}}}{\|\nabla g_{\text{eff}}\|}\right) \end{aligned} \tag{29}$$

and

$$\partial_{a\nu} g_{\text{eff}}(\boldsymbol{r}) = -\frac{12u_0}{k_{\text{B}}T}\left(R_a^{\text{vdW}}\right)^{12} g_{\text{eff}}(\boldsymbol{r})\frac{(\boldsymbol{r}-\boldsymbol{R}_a)_\nu}{\|\boldsymbol{r}-\boldsymbol{R}_a\|^{14}}\ , \tag{30}$$

such that energies, Kohn-Sham potential and forces are all defined.

V. IMPLEMENTATION AND NUMERICAL TESTS

The GPAW package[12,31] has been extended in a way that different continuum solvent models as described in Section III can be added to the DFT self-consistent cycle. GPAW uses the projector augmented wave method (PAW) devised by Blöchl[11] where the electron density and the Kohn-Sham wave functions are represented on real space grids. The use of real space grids facilitates the application of mixed boundary conditions (BC) and allows for very effective parallelization using domain decomposition[32].

In the PAW formalism, the electron density and wave functions are decomposed into a smooth part and atom centered corrections localized inside augmentation spheres. This induces a similar decomposition of the total energy into a smooth part and atom centered corrections[11,31]. The inverse power law of the potential (7) has the beneficial property

$$\lim_{\|\boldsymbol{r}-\boldsymbol{R}_a\|\to 0} u_{\text{eff}}(\boldsymbol{r}) = +\infty \qquad \forall \text{ atoms } a\ , \tag{31}$$

which together with eq. (5) ensures that the distribution function is virtually flat in the region of the solute. Therefore all solvation related fields coincide with the respective gas phase fields inside the augmentation spheres, i.e. we can assume that $\epsilon(\boldsymbol{r}) = 1$ and $g(\boldsymbol{r}) = 0$ holds for the atom centered corrections. In the framework defined in section III, we now show that the contributions to the total energy in eq. (13) arising from the presence of the solvent are functionals of the smooth part of the electron density only which simplifies the implementation greatly.

The absence of local corrections is clear for the additional interaction G_{ia} from eq. (12). It follows from the integrand f_{ia} depending only locally on the electron density and the cavity, together with the property $f_{\mathrm{ia}}|_{g=0} = 0$, which every interaction must fulfill. The disappearance of local corrections is not so obvious for the Coulomb energy E_{C}, as both the dielectric permittivity function $\epsilon(\boldsymbol{r})$ and the total charge density have a non-local effect on the electrostatic potential $\Phi(\boldsymbol{r})$. In particular, the Coulomb energy is not of the form of eq. (12). The non-locality in the Coulomb energy is usually treated by decomposing the total charge density $\rho(\boldsymbol{r})$ into a smooth part $\tilde{\rho}(\boldsymbol{r})$ and atom centered contributions

$$\rho(\boldsymbol{r}) = \tilde{\rho}(\boldsymbol{r}) + \sum_a \rho_a(\boldsymbol{r}) \tag{32}$$

in PAW[12], where every $\rho_a(\boldsymbol{r})$ is localized inside a sphere S_a around the atom's position $\boldsymbol{R}_a$ and has vanishing multipole moments with respect to a spherical multipole expansion around this position. The linearity of the Poisson equation (1) ensures that the atom centered part of the electrostatic potential does not differ from a gas phase calculation for any choice of the dielectric function as long as $\epsilon(\boldsymbol{r}) = 1$ holds inside S_a for all atoms. This is indeed the case in our model (e.g. in the the parametrization for water presented in Section VI, $g < 10^{-3}$ holds already at the van der Waals radius).

The final ingredient to the model is the Poisson solver. A parallel multi grid solver for the Poisson equation in vacuum with periodic or zero boundary conditions (BC) in any unit cell direction is already part of the GPAW package. In order to be able to solve the Poisson equation (1) in the presence of a dielectric $\epsilon(\boldsymbol{r})$, we have extended this solver to work with non-constant coefficients as outlined by Sánchez *et al.*[7].

The potential of isolated charged systems is calculated by neutralizing the system with a charge distribution, where the solution of the Poisson equation (11) is know analytically, i.e. a Gaussian charge distribution. This approach ensures that zero BC can be applied for the neutralized system despite the slow spatial decay of the $1/r$ potential. In the presence of a dielectric, we add the numerically determined charge distribution $\tilde{\rho}(\boldsymbol{r})$ centered in the simulation box corresponding to an analytical $\tilde{\Phi}(\boldsymbol{r})$ potential such that the system is neutralized in the same spirit. The resulting potential from the Poisson solver is then corrected by the known potential of the added charge distribution. Higher multipole moments are not corrected. See also Appendix B for a more detailed description of the procedure.

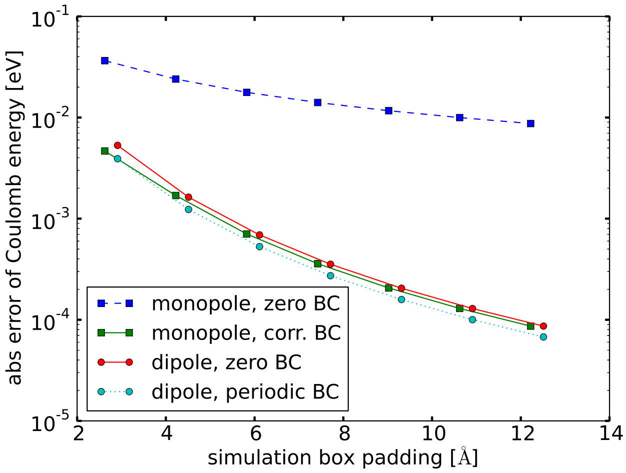

Figure 2. Absolute error of the Coulomb energy for two model charge distributions with a Gaussian dipole or monopole potential for different boundary conditions (BC). Simulation box padding is the shortest distance of the Gaussian centers to the simulation box boundary.

The accuracy of the Poisson solver is primarily limited by the size of the simulation box in isolated systems. In order to show this numerically, we have set up a model system with an effective distribution function

$$g_{\text{eff}}(\boldsymbol{r}) = 1 - \frac{G(\boldsymbol{r}, \boldsymbol{\mu}_g, \sigma)}{\max\limits_{\boldsymbol{r}} \left\{G(\boldsymbol{r}, \boldsymbol{\mu}_g, \sigma)\right\}} \tag{33}$$

and the dielectric function according to eq. (24) with $\epsilon_\infty = 80$. $G(\boldsymbol{r}, \boldsymbol{\mu}_g, \sigma)$ denotes a radially symmetric Gaussian distribution of width σ centered at $\boldsymbol{\mu}_g$. Similar to the consideration in Appendix B, we have chosen the vacuum open BC solution of a Gaussian charge distribution $\alpha\Phi_{\mathrm{G}}(\boldsymbol{r}, \boldsymbol{\mu}_\Phi, \sigma)$ with width σ centered at $\boldsymbol{\mu}_\Phi$ as a given potential and then used the charge distribution

$$\rho(\boldsymbol{r}) = -\frac{\alpha}{4\pi} \nabla \left(\epsilon(\boldsymbol{r}) \nabla \Phi_{\mathrm{G}}(\boldsymbol{r}, \boldsymbol{\mu}_\Phi, \sigma)\right) \tag{34}$$

reproducing this potential in the presence of the dielectric as the input to the Poisson solver with $\epsilon(\boldsymbol{r})$ as described above. The constant α has been chosen such that the charge distribution contained a single elementary charge. In Figure 2, we have shown the error of the Coulomb energy calculated according to eq. (10) from the solution of the Poisson solver for different BC as a function of the simulation box padding (shortest distance of the Gaussian centers to the simulation box boundary). For this purpose $\boldsymbol{\mu}_\Phi$ was chosen such that the charge distribution was placed 1 Å away from the simulation box center and we have set $\boldsymbol{\mu}_g = \boldsymbol{\mu}_\Phi$. The error has been calculated as the absolute difference to the Coulomb energy obtained by inserting the known potential $\alpha\Phi_{\mathrm{G}}(\boldsymbol{r}, \boldsymbol{\mu}_\Phi, \sigma)$ into eq. (10) which corresponds to the Coulomb energy of an open BC solution. The width σ of the Gaussian distributions has been chosen in a way that the numerical calculation of the reference Coulomb energy was not affected by the finite size of the simulation box. The distance of the Gaussian from the box boundary was greater than 12 Å for the reference calculation.

We have also constructed a dipole by placing two of these charge distributions with opposite sign and a separation of 1 Å around the center of the simulation box. The effective cavity was centered in the simulation box also. For the dipolar charge distribution, there is no noticeable difference between zero and periodic BC. When the monopole correction described in Appendix B is applied, the error for a charged system is similar to that of a neutral dipolar system as expected.

A grid spacing of 0.2 Å was used for the finest multi grid level in the above Poisson tests. Reducing the grid spacing did not reduce the error of the Coulomb energy from the Poisson solver significantly for the examined range of simulation box sizes leading us to the conclusion that the accuracy of the Poisson solver is primarily limited by the simulation box padding.

Finally, we present the numerical test of the forces including the additional contributions of eq. (30). The following computational parameters have been used for these calculations and for the rest of this work: The exchange-correlation energy was approximated by the gradient corrections proposed by Perdew, Burke and Ernzerhof (PBE)[33]. Simultaneously to the parameter estimation in Section VI, we have carefully tested the convergence of the solvation Gibbs energy of the whole model from Sections II and IV as a function of the grid spacing and simulation box padding for neutral and charged systems. A grid spacing of 0.2 Å has been chosen for the representation of the smooth wave functions. The grid spacing for the representation of the pseudo electron density as well as for all solvation related fields was always half the grid spacing of the smooth wave functions. A simulation box padding of at least 5 Å was ensured around the nuclei and we have applied zero BC for all neutral molecules and monopole corrected zero BC for all ions.

molecule	l_{min}	l_{max}	Δl	$\langle s_F \rangle$ gas phase	$\langle s_F \rangle$ water
CO	1.1	1.2	0.00125	10±2	12±1
NaCl	2.0	3.0	0.01250	2.6±0.3	3.2±0.3

Table I. Mean error $\langle s_F \rangle$ (see text) of the forces for two linear molecules in the gas phase and in water. The bond length interval and step size are given in Å and the $\langle s_F \rangle$ are given in meV Å^{-1}.

We tested the accuracy of the forces for the molecules CO and NaCl in the presence of water. We have used the parameters for water from Section VI and varied the bond length l of the molecules around the gas phase optimum. The error has been estimated as

$$s_F(l) = \left| \frac{|F_1(l)| + |F_2(l)|}{2} - \frac{\partial E(l)}{\partial l} \right|, \tag{35}$$

where F_a is the force component of atom a along the molecule's axis and $\frac{\partial E(l)}{\partial l}$ has been evaluated from a five point central finite difference. Table I lists the error averaged over the tested bond lengths for both molecules in the gas phase and in water. The standard deviation of the mean is given as an uncertainty. There is no significant difference between the errors of the forces of a gas phase calculation and a calculation within the CSM establishing the good accuracy of the forces.

VI. PARAMETRIZATION FOR WATER

Water is arguably the most important solvent in particular for biological systems. It's high dielectric permittivity also makes it a prime example for the application of a polarizable continuum model[2].

The first step in the application of our model is to fix the single parameter u_0 of the effective repulsive potential that controls the size of the cavity. The parameter u_0 is required to minimize the mean absolute error (MAE) between the left hand side and right hand side of

$$\int \big(1 - g_{\text{eff}}[u_{\text{eff}}(u_0, \boldsymbol{r})]\big) \mathrm{d}\boldsymbol{r} = \overline{v}_M^{\infty} - \kappa_T k_{\text{B}} T \tag{36}$$

for a chosen training set of molecules. We use the experimental partial molar volumes at infinite dilution of seven neutral molecules[34] at $T = 298\,\text{K}$ from the literature[15–20] for this purpose. The experimental isothermal compressibility of water[35] $\kappa_T = 4.53 \times 10^{-10}\,\mathrm{Pa}^{-1}$, and van der Waals radii from Bondi[36] have been applied. The only exception is hydrogen, where a van der Waals radius of 1.09 Å as suggested by Rowland and Taylor[37] has been used. The structures were collected from PubChem[38] and relaxed in the gas phase without any symmetry constraints.

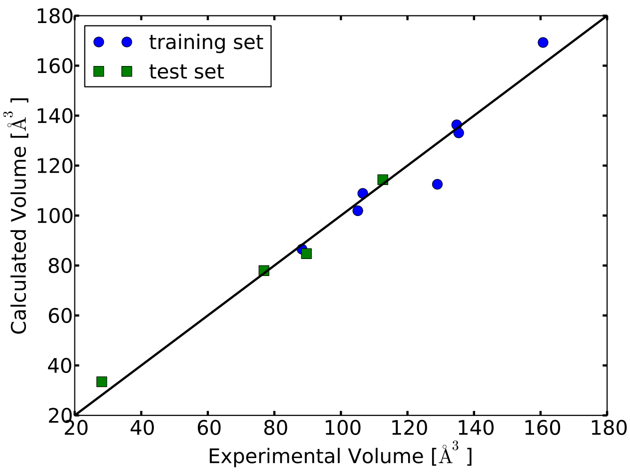

Figure 3. Calculated versus experimental partial molar volumes $\overline{v}_M^\infty - \kappa_T k_\mathrm{B} T$ for the optimal choice $u_0 = 180\,\mathrm{meV}$ of the training set and a test set of four other neutral molecules in water at $T = 298\,\mathrm{K}$.

The best fit within this training set is obtained for $u_0 = 180\,\mathrm{meV} (\widehat{=} 17\,\mathrm{kJ\,mol}^{-1})$ and results in the small mean absolute error of 5.1 Å^3 as depicted in Figure 3. As a first test of the generality of our approach, the partial volumes of four additional molecules, namely water, acetonitrile, ethanol and DMSO (ordered by ascending volume) have been also included in Figure 3. Experimental data has been obtained from Refs. 16, 19, and 39 and the molar volume of water has been calculated from its bulk density. The excellent agreement between experimental and calculated volumes shows the relevance of our model and that the fitted u_0 is also a good choice for other molecules.

In a next step, we have compared solvation Gibbs energies calculated according to

$$\Delta G_\mathrm{S}^* = \Delta G_\mathrm{el} + \gamma A \tag{37}$$

for the whole training set of 13 small neutral molecules in water from Ref. 9 to experimental solvation Gibbs energies. The value of $\epsilon_\infty = 78.36$ was used for the dielectric constant of water[40]. A choice of $\gamma = 18.4\,\mathrm{dyn\,cm}^{-1}$ minimizes the mean absolute error for the training set to be 4.3 kJ mol^{-1}. This value is substantially lower than the surface tension[41] $\gamma_{H_2O} = 72\,\mathrm{dyn\,cm^{-1}}$ of water at 298 K as it also contains the attractive interaction between solute and solvent. We only allowed the structures to relax in the gas phase and used the same geometry for the liquid phase. Relaxing the structures further in solution did not reveal notable changes in the solvation Gibbs energies for this particular training set.

The optimal value of γ is in agreement with what would be expected from more sophisticated calculations of the dispersion and repulsion contributions: Amovilli and Mennucci[27] have presented a method to calculate G_{rep} and G_{disp} in the framework of the PCM[4] model. They have listed their calculated results for G_{rep}, G_{disp} and G_{cav} for 20 neutral molecules in water in Ref. 27 yielding

$$\left\langle \frac{G_{\mathrm{cav}} + G_{\mathrm{rep}} + G_{\mathrm{dis}}}{G_{\mathrm{cav}}} \right\rangle \gamma_{H_2O} = (20.6 \pm 1.7)\,\mathrm{dyn\,cm^{-1}}. \tag{38}$$

Having fixed the two parameters $u_0 = 180\,\mathrm{meV}(\widehat{=}19\,\mathrm{kJ\,mol^{-1}})$ and $\gamma = 18.4\,\mathrm{dyn\,cm^{-1}}$, we have compared calculated solvation Gibbs energies to experimental data for neutral molecules, cations and anions in a test set disjoint from the training set. The test set consisted of 97 neutral molecules, 52 cations and 56 anions compiled by Kelly *et al.*[42] where monoatomic ions have been excluded. We have chosen this test set including ions as the performance of CSMs with a smooth cavity for ions is of fundamental interest for the application in many fields of chemistry[43].

	Neutrals	Cations	Anions
MAE	4.8	12.6	45.1
RMS	6.6	18.7	51.0
MSE	1.4	3.2	45.1

Table II. Mean absolute error, root mean square and mean signed error for calculated solvation Gibbs energies in water compared to experimental values. All values in kJ mol^{-1}.

Table II lists the accuracy of this parametrization for water. A more detailed comparison between calculated and experimental values along with a histogram of the (signed) error is shown in Figures 4, 5 and 6. The neutral molecules exhibit a mean absolute error of 4.8 kJ mol^{-1} which is in agreement with the value from the training set and comparable to other continuum solvent implementations with a smooth cavity[9,10]. A mean absolute error of 2.3 kJ mol^{-1} for neutral molecules is achieved by the state of the art SM6 implementation with the expense of introducing many more parameters[44]. The cations also exhibit a moderate MAE of 12.6 kJ mol^{-1} similar to the errors reported by Dziedzic *et al.* for a smooth cavity defined through a fixed iso-density surface[10] and the self-consistent approach by Dupont *et al.*[43]. A similar mean absolute error of 11.4 kJ mol^{-1} is reported[43] for cations in the SM6 model. Both neutral species and cations exhibit a mean signed error close to zero.

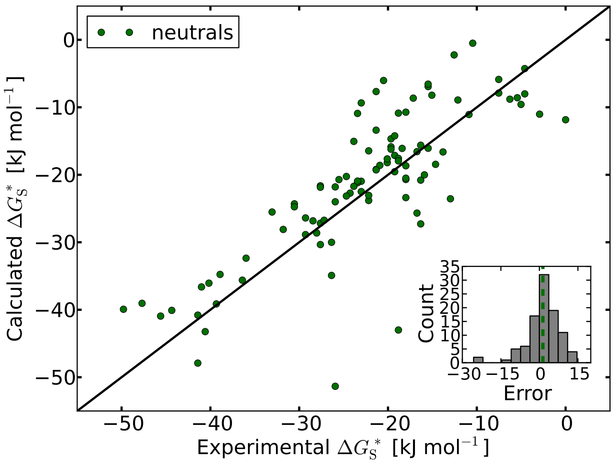

Figure 4. Calculated values of ΔG_{S}^* according to eq. (37) versus experimental absolute aqueous solvation Gibbs energies for 97 neutral molecules disjoint from the training set. Embedded plot: Histogram of the signed error of the calculated values. The mean signed error is shown as a dashed vertical line in the embedded plot.

The situation is different for anions. Here the model underestimates the solvation effect as can be seen from the mean signed error of +45.1 kJ mol^{-1}. This effect is also in agreement with the errors reported in the work of Dziedzic *et al.*[10] and Dupont *et al.* (for the parameters fitted to neutral molecules)[43]. A mean absolute error of 14.9 kJ mol^{-1} is reported[43] for anions in the highly parametrized SM6 model. The cause of this underestimation of the solvation effect is well known in the literature[45–54] and results from short-range solvent-solute interactions, such as hydrogen bonding and the reorientation of water molecules in the first solvation shell, effectively reducing the cavity size for anions. As we do not consider orientational degrees of freedom in our distribution function $g_{\mathrm{eff}}(\boldsymbol{r})$ which is merely a function of the location of the solvent molecules and we do not treat hydrogen bonding explicitly, the

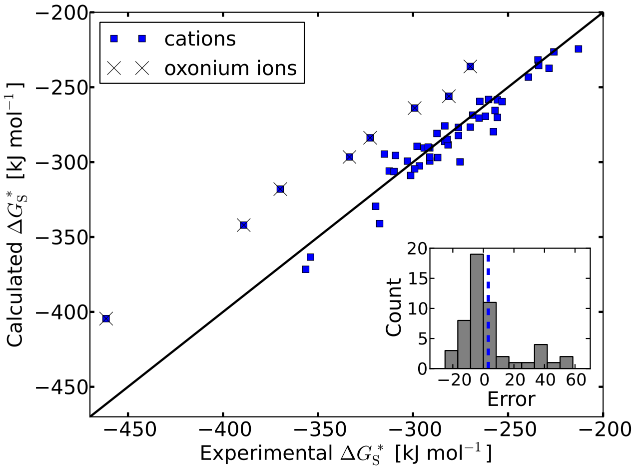

Figure 5. Same as Figure 4 but for 52 cations.

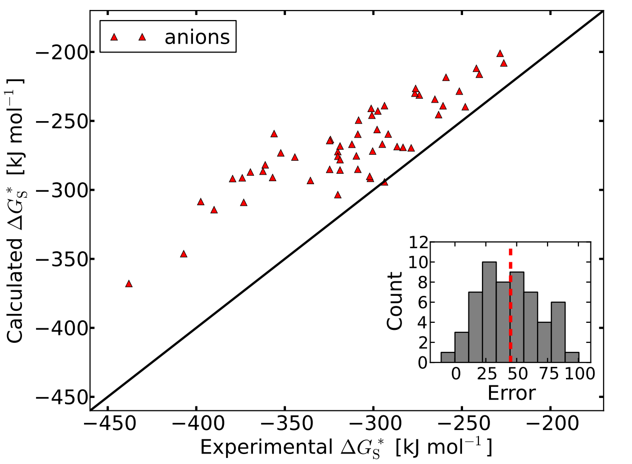

Figure 6. Same as Figure 4 but for 56 anions.

model cannot reproduce this charge asymmetry without further modification[54,55].

Arguing consistently, one would expect an overestimation of the solvation effect for cations due to the reorientation of water molecules. This trend is is indeed visible in Figure 5 with the exception of eight oxonium ions where the solvation effect is underestimated by around 40 kJ mol^{-1}. Excluding these molecules, the mean signed error changes from +3.2 kJ mol^{-1} to −3.6 kJ mol^{-1} and the mean absolute error is reduced to 7.5 kJ mol^{-1}. We suspect that the underestimation of the solvation effect for the oxonium ions is due to the lack of an explicit description of hydrogen bonds[56].

VII. OTHER SOLVENTS

The procedure described in Section VI for finding the optimal parameters u_0 and γ can in principle be applied to other solvents. In the current state, the model is primarily designed for polar solvents. In Section III we have outlined, how other terms than the surface term for the non-polar interaction or the cavity formation energy can in principle be included in order to extend the model to solvents where G_{ia} predominates.

To our knowledge, there is little published data on the performance of CSMs with a smooth cavity for other solvents than water. We have applied the optimization scheme from Section VI to the solvent dimethyl sulfoxide (DMSO). The optimization of the parameter u_0 controlling the cavity size was restricted to the pure solvent. In that case, only the bulk density and the isothermal compressibility of DMSO are needed. These experimental quantities have been obtained from Refs. 57 and 58 at $T = 298\,\mathrm{K}$. The resulting value for u_0 was $200\,\mathrm{meV}(\widehat{=}19\,\mathrm{kJ\,mol^{-1}})$ and therefore remarkably near to the value of water. The experimental dielectric constant of $\epsilon_\infty = 47.2$ of DMSO[59] was used.

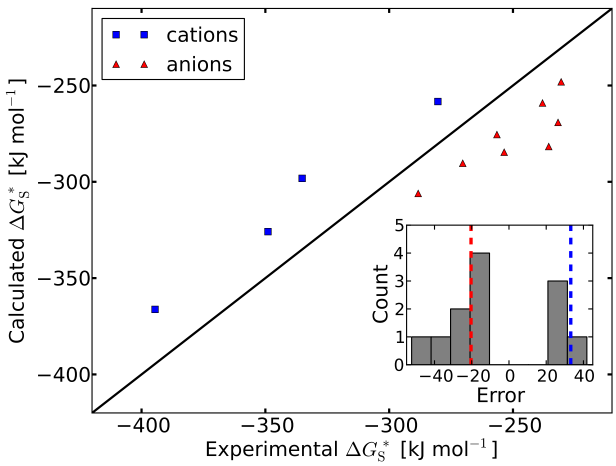

Figure 7. Calculated values of ΔG^*_S according to eq. (37) versus experimental absolute solvation Gibbs energies in DMSO for four cations and eight anions disjoint from the training set. Embedded plot: Histogram of the signed error of the calculated values. The mean signed error (MSE) is shown as a dashed vertical line in the embedded plot for cations (positive MSE) and anions (negative MSE).

The mean absolute error of calculated solvation Gibbs energies compared to reference values of seven neutral molecules in DMSO[60] was minimized at $\gamma = 8.8\,\mathrm{dyn\,cm^{-1}}$. The value of the mean absolute error for the neutral training set was $7.2\,\mathrm{kJ\,mol^{-1}}$. As a test we have compared calculated and experimental solvation Gibbs energies of four cations and eight anions[61] as shown in Figure 7. Monoatomic ions were not included in the test.

There is a reasonable agreement between calculated and experimental solvation Gibbs energies. Judging from the small test set, the cation/anion asymmetry in DMSO is opposite to that of water. This is also expected, DMSO being a dipolar aprotic solvent compared to water as a protic solvent[53,62].

VIII. APPLICATIONS

In this section we present two applications within the solvent DMSO and the simulation of the polar part of the electrostatic screening for a charged gold cluster in an ionic liquid.

A. Spiropyrans

Prior to the implementation of the model described in Sections II and IV, the model based on a smooth cavity defined through atomic radii from Sánchez *et al.*[7] had already been incorporated into the GPAW code by us. We applied the model for the calculation of isomerization energies of spiropyrans in DMSO[63]. Spiropyrans are multi-responsive chromophores. Usually the closed spiropyran (SP) form is energetically preferred, but the transformation to the meta-stable open merocyanine (MC) form can be enforced by light or mechanical force[64]. The MC form has a larger dipole moment and therefore the energetical gap to the SP form reduces in polarizable media. Through pH alternation, also the protonated merocyanine (MCH^+) form occurs, having considerably different optical properties than the MC form[63].

In the model of Sánchez *et al.*, the only free parameter β of the cavity controls the steepness of the transition region, while the size of the cavity is fixed by van der Waals radii. In the original work[7], this parameter has been tuned to describe both the polar and non-polar interactions in water resulting in a value of $\beta = 2.4$. We were not able to reproduce their reported value for the solvation Gibbs energy of a water molecule in water with this choice of β in the GPAW implementation[65]. We have not further investigated the source of this discrepancy, but have varied the parameter β to match only the polar contribution resulting in a value of $\beta = 6.4$ for the GPAW implementation. Within this choice of β, the transition region of the cavity is so steep that it changes from 0 to 1 within a few grid points affecting the numerical stability of the forces markedly. For this reason, we review the computational results from Ref. 63 by applying our present model from Sections II and IV to the same molecules.

form	E_{NO_2}	E_{PhOMe}	$E_{PhOMe} - E_{NO_2}$
SP	0	0	0
MC	0.16^a 0.03^b	-0.01^a -0.14^b	-0.17^a -0.11^b
MCH^+	0.12^a -0.29^b	-0.42^a -0.71^b	-0.54^a -0.42^b

Table III. Energies of the different spiropyran forms in DMSO relative to the SP form as a function of the side group. ^{a}Ref. 63, ^{b}this work. All values are given in eV ($1\,\mathrm{eV} \mathrel{\widehat{=}} 96.485\,\mathrm{kJ\,mol^{-1}}$).

One of the main computational results of Ref. 63 was the stabilization of the MCH^+ form in the solvent DMSO as a function of the side group. We have re-evaluated the simulated energy differences between the SP, MC and MCH^+ forms in DMSO with the parametrization for DMSO from Section VII. A grid spacing of 0.18 Å was used for the representation of the smooth wave functions. The detailed procedure for the calculation of the energies is described in Ref. 63. Table III compares the simulated energies from Ref. 63 and from the present model. Good qualitative agreement with slight quantitative differences is found. The stabilization of the MCH^+ form through the phenyl-based side group (PhOMe) is also present in our new model. The absolute differences between the energies from the two models for the MC and MCH^+ form for the same side group lie within the errors expected for the solvation Gibbs energy of cations in DMSO (compare Figure 7). Therefore it is hard to judge which of the models is in better agreement to the experiment without further data.

B. Proton transfer

As a second application we have simulated the proton transfer from Bis(trifluormethanesulfonyl)imide ($HNTf_2$) to DMSO with DMSO as a solvent by performing a structural optimization from the forces in solution. Strong evidence for the formation of a NTf_2^--DMSO-H^+ contact ion pair in DMSO is reported by the group of I. Krossing[66]. In this reaction, the proton is transferred from the nitrogen atom in $HNTf_2$ to the oxygen atom in DMSO, forming a contact ion pair from the overall neutral adduct.

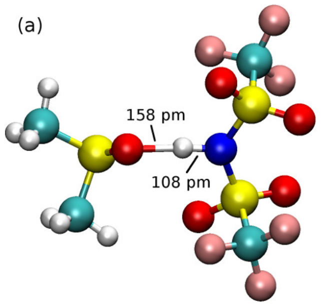

Figure 8. Relaxed structure of a $HNTf_2$-DMSO pair in the gas phase (a) and in DMSO (b). In the gas phase, the proton is closer to the nitrogen of NTf_2^- whereas in DMSO, it is closer to the oxygen of DMSO. Gray: hydrogen, turquoise: carbon, yellow: sulfur, red: oxygen, blue: nitrogen, pink: fluorine (colors online)

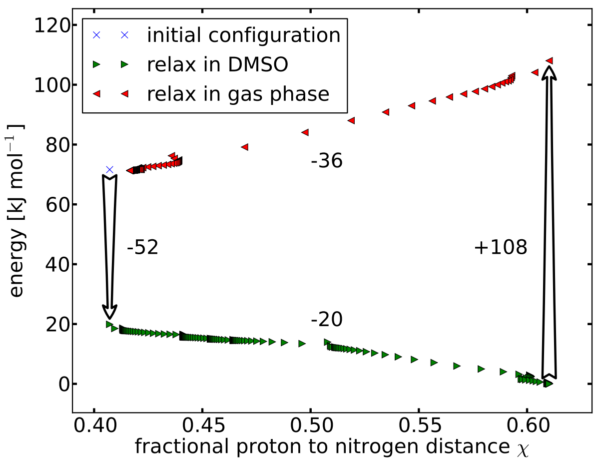

Figure 9. Relaxation cycle of a $HNTf_2$-DMSO pair in DMSO and the gas phase. The energy as a function of the fractional distance χ (eq. (39)) of the proton to the nitrogen in NTf_2^- is shown. The vertical arrows denote the transitions from the gas phase to DMSO and back. The according energy differences for the transition and the relaxation are indicated besides the arrows and the markers (in $\mathrm{kJ\,mol^{-1}}$). The initial configuration is the relaxed gas phase structure.

Starting from the relaxed gas phase geometry, the structure was relaxed in DMSO and then again in the gas phase, returning to the initial configuration. We have used the FIRE algorithm[67] for the structural optimization. Its convergence-criterion for the relaxation is $\max_{\text{atoms}\,a} \|\boldsymbol{F}_a\| < f_{\max}$. Before the proton is transferred in solution, the maximum force on any atom drops down to $0.02\,\mathrm{eV\,\AA^{-1}}$. Nevertheless, the forces are accurate enough for the relaxation to take place. The relaxations were aborted at $f_{\max} = 0.01\,\mathrm{eV\,\AA^{-1}}$ both in solution and in the gas phase. We have found no energy barrier for this process such that the local structure optimization was able to capture the proton transfer. This cycle is shown in Figure 9, where we have used the fractional distance of the proton to the nitrogen in NTf_2^-

$$\chi = \frac{\|\boldsymbol{r}_{H^+} - \boldsymbol{r}_N\|}{\|\boldsymbol{r}_{H^+} - \boldsymbol{r}_N\| + \|\boldsymbol{r}_{H^+} - \boldsymbol{r}_O\|} \tag{39}$$

as the reaction coordinate. The vectors $\boldsymbol{r}_X, X = H^+, O, N$ denote positions of the atoms (see also Figure 8). The "vertical" solvation Gibbs energies are $-52\,\mathrm{kJ\,mol^{-1}}$ for the neutral adduct and $-108\,\mathrm{kJ\,mol^{-1}}$ for the ion pair. The difference between these values can be attributed to the larger charge separation in the ion pair that is stabilized in the solvent. The "relaxed" solvation Gibbs energy starting from the neutral adduct in the gas phase ending up with the ion pair in DMSO is $-72\,\mathrm{kJ\,mol^{-1}}$ and the energy decrease during optimization in DMSO is $20\,\mathrm{kJ\,mol^{-1}}$ in our model. Ref. 66 finds values in the range of $42\,\mathrm{kJ\,mol^{-1}}$ to $68\,\mathrm{kJ\,mol^{-1}}$ for the energy decrease depending on the solvation model, basis sets and functionals. Despite the rather large variation of the energy decrease during optimization between different models, the proton transfer is found ubiquitously.

C. Charging of gold clusters

As a third application, we have investigated the change in the capacitance of a gold nanoparticle induced by the polar part of the interaction with an ionic liquid compared to the gas phase. In particular we have studied an Au_{39} cluster in the ionic liquid $[BMIm][BF_4]$[68] supplemental to the work done in Refs. 69 and 70.

Similar to the parametrization for DMSO described in Section VII, we have only used the density and the isothermal compressibility of the pure solvent (the ionic liquid) for the determination of the parameter u_0. We have chosen u_0 such that the combined volume of $BMIm^+$ and BF_4^- calculated from the respective cavities of the gas phase relaxed structures matches the experimental term $\overline{v}_M^\infty - \kappa_T k_\mathrm{B} T$, where $\overline{v}_M^\infty$ has been calculated from the density of the pure liquid. Experimental quantities have been obtained from Refs. 71 and 72. The resulting value was $u_0 = 160\,\mathrm{meV}(\widehat{=}15\,\mathrm{kJ\,mol^{-1}})$ at $T = 298\,\mathrm{K}$.

The cluster capacitance at charge state z is evaluated as the finite difference expression[70]

$$C(z) = \frac{e^2}{E(z+1) - 2E(z) + E(z-1)}, \tag{40}$$

where $E(z)$ is the energy of the cluster at charge state z. Structure relaxation does not contribute significantly to the z-dependence[70]. Therefore we have used the $z = 0$ gas phase relaxed structure for all charge states. The determination of the surface term is not needed in the calculation of the cluster capacitance as these terms do not depend on z. The experimental dielectric constant of $\epsilon_\infty = 11.7$ was used for [BMIm][BF_4][69].

z	DFT gas phase	DFT + CSM	experimental
0	0.07	0.47	1.20
+3	0.06	0.44	0.56

Table IV. Calculated and experimental charge dependent capacitance of a gold cluster in aF = 10^{-18}F. Calculated: Au_{39}, structure as in Ref. 70, experimental: Ref. 69

Table IV lists the calculated charge dependent capacitance in the gas phase and with our CSM for the charge states $z = 0$ and $z = +3$ along with the experimentally measured capacitance of gold clusters in [BMIm][BF_4] of similar size[69]. While the gas-phase capacitance is more than a magnitude smaller than in the experiment, the value of the CSM model is in a similar range. We note, that the capacitance within the CSM model is not simply the gas phase capacitance times the dielectric constant, which would lead to 0.7 aF[69], as the dielectric screening is not fully present at the location of the excess charge on the cluster surface.

The high experimental capacitance at charge state $z = 0$ has been explained by explicit re-orientation of the ions around the cluster[69,70] that is not included in the CSM model. The reorientation of the ions around the cluster is almost saturated at charge state $z = +3$, such that the dielectric screening arises mainly from the polar part of the interaction. This is in line with the fact, that the calculated cluster capacitance from the CSM and the experimental value for $z = +3$ are similar.

IX. CONCLUSIONS

We have presented a continuum solvent model with a smooth cavity parametrized to match experimental partial molar volumes at infinite dilution. The resulting cavity is used to describe the polar solvent-solute interaction by a polarizable medium with the experimental dielectric constant of the solvent as an ingredient. Non-polar interactions and the cavity formation energy are described as a geometric term proportional to a particular choice of the cavity surface area. The proportionality constant is fitted to match experimental solvation Gibbs energies. The accuracy of the predicted aqueous solvation Gibbs energies is similar to other CSMs with a cavity defined as a smooth function of the electron density (iso-density approaches).

The effective potential $u_{\text{eff}}(\boldsymbol{r})$ and the cavity $g_{\text{eff}}(\boldsymbol{r})$ have a direct physical interpretation in contrast to the mathematical step functions often employed in other models. The cavity is defined via experimental data not connected to solvation energetics, but based on volumetric measurements. Our cavity model therefore helps to separate the contributions from the polarizable medium and short-range effects in the framework of CSMs with a smooth cavity.

There are several possibilities to further improve our model by introducing higher complexity. In the present work, we have modeled the non-polar short-range effects only coarsely through the cavity surface area which results in the inability to reproduce the cation/anion asymmetry observed in different solvents. This problem is also known in iso-density models for a fixed parametrization[10,43]. Possible solutions are the treatment of short-range effects as recently proposed by Pomogaeva and Chipman[54,55], the insertion of explicit solvent molecules as in the cluster continuum model[73,74] or the re-parametrization depending on the charge states of the solute[43].

Barone *et al.*[75] have demonstrated how the inaccuracies of CSMs can be overcome for implementations using the homogeneous approximation by replacing the standard van der Waals radii with a set of highly parametrized united atom radii. To our knowledge, this high level of customization has not been applied yet for CSMs with a smooth cavity. A possible approach within our model could be the inclusion of the UAHF radii[75] instead of the the standard van der Waals radii into the definition of the effective potential $u_{\text{eff}}(\boldsymbol{r})$. It is not clear, whether the accuracy in the description of experimental partial molar volumes could be retained in that case, however.

ACKNOWLEDGMENTS

We thank the group of I. Krossing and especially D. Himmel for kindly providing the example of Section VIII B prior to publication as well as for stimulating discussion about solvation phenomena. Computational resources from FZ-Jülich and the BWGrid initiative[76]

are gratefully acknowledged.

Appendix A: Cavity surface area

Let $n(\boldsymbol{r})$ be the electron density and $\vartheta(n(\boldsymbol{r}))$ a smooth step function as in Ref. 9. Correcting the sign error, the cavity surface area is defined by Andreussi *et al.*[9] (eq. (63)) as

$$A_\Delta = \int \left(\vartheta\left(n(\boldsymbol{r}) + \frac{\Delta}{2}\right) - \vartheta\left(n(\boldsymbol{r}) - \frac{\Delta}{2}\right)\right) \times \frac{\|\nabla n(\boldsymbol{r})\|}{\Delta} \mathrm{d}\boldsymbol{r} \tag{A1}$$

for Δ a finite difference parameter. Setting $g = 1 - \vartheta$, we arrive at

$$A_\Delta = -\int \frac{g\left(n(\boldsymbol{r}) + \frac{\Delta}{2}\right) - g\left(n(\boldsymbol{r}) - \frac{\Delta}{2}\right)}{\Delta} \|\nabla n(\boldsymbol{r})\| \,\mathrm{d}\boldsymbol{r} \tag{A2}$$

The fraction in eq. (A2) is the central difference quotient for a fixed value of $\boldsymbol{r}$. Taking the limit $\Delta \to 0$ yields

$$\lim_{\Delta\to 0} A_\Delta = \int \|\nabla g(\boldsymbol{r})\| \,\mathrm{d}\boldsymbol{r}, \tag{A3}$$

where we have used $\frac{\mathrm{d}g}{\mathrm{d}n} = -\frac{\mathrm{d}\vartheta}{\mathrm{d}n} \leq 0$, the chain rule and the identification $g(\boldsymbol{r}) = g(n(\boldsymbol{r}))$.

Let $g_{\mathrm{eff}}(\boldsymbol{r})$ be the effective cavity from Section II. For a single atom at the origin with van der Waals radius R_a, g_{eff} is merely a function of the distance $r = \|\boldsymbol{r}\|$ from the origin:

$$g_{\mathrm{eff}}(r) = \exp\left(-\beta u_0 \left(\frac{R_a}{r}\right)^{12}\right) \tag{A4}$$

with $\beta = \frac{1}{k_{\mathrm{B}}T}$. Due to the spherical symmetry, we have

$$\begin{aligned} A[g_{\mathrm{eff}}] &= \int \|\nabla g_{\mathrm{eff}}\| \,\mathrm{d}\boldsymbol{r} = 4\pi \int_{r=0}^{\infty} r^2 \frac{\partial g_{\mathrm{eff}}(r)}{\partial r} \mathrm{d}r \\ &= 4\pi \sqrt[6]{\beta u_0} R_a^2 \Gamma(\frac{5}{6}) \end{aligned} \tag{A5}$$

and since in that case all isosurfaces are spheres centered at the origin, the according isovalue is

$$g_{\mathrm{eff}}\left(\sqrt[12]{\beta u_0} R_a \sqrt{\Gamma(\frac{5}{6})}\right) = \exp\left(-\Gamma(\frac{5}{6})^{-6}\right) \approx 0.62 \tag{A6}$$

independent of β, u_0 and R_a.

Appendix B: Charged systems

The Coulomb potential of systems with a non-zero total charge $Q = \int \rho(\boldsymbol{r})\mathrm{d}\boldsymbol{r}$ does not decay fast enough for zero boundary conditions (BC) to be a good approximation to open BC for reasonable simulation box sizes. For calculations in the gas phase, a Gaussian charge distribution is therefore added to the total charge density such that the monopole is neutralized. Due to the linearity of the Poisson equation, the slowly decaying potential of this extra charge distribution can then simply be subtracted from the zero BC multi grid solution of the neutralized system. For $\epsilon(\boldsymbol{r}) = 1$, the solution Φ_{G} of the Poisson equation (1) is analytically known for a Gaussian charge distribution and open BC. The integration constant for open BC is chosen such that the potential vanishes at infinite distance to the localized charge distribution.

This numerical trick is not possible anymore in this form for an arbitrary dielectric function $\epsilon(\boldsymbol{r})$, since then the potential of a Gaussian charge distribution is not known. In that case, we add a charge distribution

$$\rho_\epsilon(\boldsymbol{r}) = -\frac{\alpha}{4\pi}\nabla\left(\epsilon(\boldsymbol{r})\nabla\Phi_{\mathrm{G}}(\boldsymbol{r})\right) \tag{B1}$$

with Φ_{G} the open BC vacuum solution of a Gaussian charge distribution. The constant α is given by

$$\alpha = \frac{4\pi Q}{\int \nabla\left(\epsilon(\boldsymbol{r})\nabla\Phi_{\mathrm{G}}(\boldsymbol{r})\right)\mathrm{d}\boldsymbol{r}}, \tag{B2}$$

such that

$$\int \rho_\epsilon(\boldsymbol{r})\mathrm{d}\boldsymbol{r} = -Q. \tag{B3}$$

The potential of ρ_ϵ for open BC in presence of the dielectric is then $\alpha\Phi_{\mathrm{G}}$ by definition and we can proceed as in the gas phase case.

REFERENCES

[1]H. M. Senn and W. Thiel, Angew. Chem., Int. Ed. **48**, 1198 (2009).

[2]J. Tomasi, B. Mennucci, and R. Cammi, Chem. Rev. **105**, 2999 (2005).

[3]F. M. Floris, J. Tomasi, and J. L. P. Ahuir, J. Comput. Chem. **12**, 784 (1991).

[4]S. Miertuš, E. Scrocco, and J. Tomasi, Chem. Phys. **55**, 117 (1981).

[5]J.-L. Fattebert and F. Gygi, J. Comput. Chem. **23**, 662 (2002).

[6]W. Im, D. Beglov, and B. Roux, Comput. Phys. Commun. **111**, 59 (1998).

[7]V. M. Sánchez, M. Sued, and D. A. Scherlis, J. Chem. Phys. **131**, 174108 (2009).

[8]D. A. Scherlis, J.-L. Fattebert, F. Gygi, M. Cococcioni, and N. Marzari, J. Chem. Phys. **124**, 074103 (2006).

[9]O. Andreussi, I. Dabo, and N. Marzari, J. Chem. Phys. **136**, 064102 (2012).

[10]J. Dziedzic, H. H. Helal, C.-K. Skylaris, A. A. Mostofi, and M. C. Payne, Europhys. Lett. **95**, 43001 (2011).

[11]P. E. Blöchl, Phys. Rev. B **50**, 17953 (1994).

[12]J. J. Mortensen, L. B. Hansen, and K. W. Jacobsen, Phys. Rev. B **71**, 035109 (2005).

[13]J. G. Kirkwood and F. P. Buff, J. Chem. Phys. **19**, 774 (1951).

[14]M. Ohba, F. Kawaizumi, and H. Nomura, J. Phys. Chem. **96**, 5129 (1992).

[15]C. Pettenati, P. Alessi, M. Fermeglia, and I. Kikic, Thermochim. Acta **162**, 203 (1990).

[16]S. Hovorka, A. Roux, G. Roux-Desgranges, and V. Dohnal, J. Solution Chem. **28**, 1289 (1999).

[17]L. Hnedkovsky and I. Cibulka, J. Chem. Thermodyn. **35**, 1185 (2003).

[18]J. C. Moore, R. Battino, T. R. Rettich, Y. P. Handa, and E. Wilhelm, J. Chem. Eng. Data **27**, 22 (1982).

[19]J. T. Edward, P. G. Farrell, and F. Shahidi, J. Chem. Soc., Faraday Trans. 1 **73**, 705 (1977).

[20]F. Shahidi, P. G. Farrell, and J. T. Edward, J. Chem. Soc., Faraday Trans. 1 **73**, 715 (1977).

[21]J. G. Kirkwood, J. Chem. Phys. **7**, 919 (1939).

[22]J. N. Murrell, M. Randic, and D. R. Williams, Proc. R. Soc. London, Ser. A **284**, 566 (1965).

[23]J. H. Jensen and M. S. Gordon, Mol. Phys. **89**, 1313 (1996).

[24]J. H. Jensen and M. S. Gordon, J. Chem. Phys. **108**, 4772 (1998).

[25]A. Ben-Naim, J. Solution Chem. **30**, 475 (2001).

[26]W. Kohn and L. J. Sham, Phys. Rev. **140**, A1133 (1965).

[27]C. Amovilli and B. Mennucci, J. Phys. Chem. B **101**, 1051 (1997).

[28]The functional should also change in the presence of a dielectric as the exchange-energy is modified if $\epsilon \neq 1$. This discussion is out of scope of the present work, however.

[29]U. Bordoloi and H.-W. Shen, in *IEEE Visualization 2003* (2003) pp. 201–208.

[30]Y. Livnat, H.-W. Shen, and C. Johnson, IEEE Trans. Vis. Comput. Graph. **2**, 73 (1996).
[31]J. Enkovaara, C. Rostgaard, J. J. Mortensen, J. Chen, M. Dułak, L. Ferrighi, J. Gavnholt, C. Glinsvad, V. Haikola, H. A. Hansen, H. H. Kristoffersen, M. Kuisma, A. H. Larsen, L. Lehtovaara, M. Ljungberg, O. Lopez-Acevedo, P. G. Moses, J. Ojanen, T. Olsen, V. Petzold, N. A. Romero, J. Stausholm-Møller, M. Strange, G. A. Tritsaris, M. Vanin, M. Walter, B. Hammer, H. Häkkinen, G. K. H. Madsen, R. M. Nieminen, J. K. Nørskov, M. Puska, T. T. Rantala, J. Schiøtz, K. S. Thygesen, and K. W. Jacobsen, J. Phys.: Condens. Matter **22**, 253202 (2010).
[32]J. Enkovaara, N. A. Romero, S. Shende, and J. J. Mortensen, Procedia Comput. Sci. **4**, 17 (2011).
[33]J. P. Perdew, K. Burke, and M. Ernzerhof, Phys. Rev. Lett. **77**, 3865 (1996).
[34]Mol 013, 016, 090, 140, 160, 200, 206 from Ref. 9.
[35]A. J. Easteal and L. A. Woolf, J. Chem. Thermodyn. **20**, 693 (1988).
[36]A. Bondi, J. Phys. Chem. **68**, 441 (1964).
[37]R. S. Rowland and R. Taylor, J. Phys. Chem. **100**, 7384 (1996).
[38]E. E. Bolton, Y. Wang, P. A. Thiessen, and S. H. Bryant, in *Annu. Rep. Comput. Chem.*, Vol. 4, edited by R. A. Wheeler and D. C. Spellmeyer (Elsevier, 2008) Chap. 12, pp. 217–241.
[39]C. De Visser, W. J. M. Heuvelsland, L. A. Dunn, and G. Somsen, J. Chem. Soc., Faraday Trans. 1 **74**, 1159 (1978).
[40]J.-L. Fattebert and F. Gygi, Int. J. Quant. Chem. **93**, 139 (2003).
[41]N. B. Vargaftik, B. N. Volkov, and L. D. Voljak, J. Phys. Chem. Ref. Data **12**, 817 (1983).
[42]C. P. Kelly, C. J. Cramer, and D. G. Truhlar, J. Phys. Chem. B **110**, 16066 (2006).
[43]C. Dupont, O. Andreussi, and N. Marzari, J. Chem. Phys. **139**, 214110 (2013).
[44]C. P. Kelly, C. J. Cramer, and D. G. Truhlar, J. Chem. Theory Comput. **1**, 1133 (2005).
[45]D. L. Mobley, A. E. Barber, C. J. Fennell, and K. A. Dill, J. Phys. Chem. B **112**, 2405 (2008).
[46]W. M. Latimer, K. S. Pitzer, and C. M. Slansky, J. Chem. Phys. **7**, 108 (1939).
[47]A. A. Rashin and B. Honig, J. Phys. Chem. **89**, 5588 (1985).
[48]B. Roux, H. A. Yu, and M. Karplus, J. Phys. Chem. **94**, 4683 (1990).
[49]G. Hummer, L. R. Pratt, and A. E. García, J. Phys. Chem. **100**, 1206 (1996).
[50]R. M. Lynden-Bell and J. C. Rasaiah, J. Chem. Phys. **107**, 1981 (1997).

[51]S. Koneshan, J. C. Rasaiah, R. M. Lynden-Bell, and S. H. Lee, J. Phys. Chem. B **102**, 4193 (1998).
[52]H. S. Ashbaugh, J. Phys. Chem. B **104**, 7235 (2000).
[53]A. J. Parker, Q. Rev. Chem. Soc. **16**, 163 (1962).
[54]A. Pomogaeva and D. M. Chipman, J. Chem. Theory Comput. **7**, 3952 (2011).
[55]A. Pomogaeva and D. M. Chipman, J. Chem. Theory Comput. **10**, 211 (2014).
[56]M. Meot-Ner (Mautner), Chem. Rev. **105**, 213 (2005).
[57]P. S. Nikam, M. C. Jadhav, and M. Hasan, J. Chem. Eng. Data **41**, 1028 (1996).
[58]G. I. Egorov, D. M. Makarov, and A. M. Kolker, J. Chem. Eng. Data **55**, 3481 (2010).
[59]S. E. McLain, A. K. Soper, and A. Luzar, J. Chem. Phys. **124**, 074502 (2006).
[60]A. V. Marenich, C. J. Cramer, and D. G. Truhlar, J. Phys. Chem. B **113**, 6378 (2009).
[61]C. P. Kelly, C. J. Cramer, and D. G. Truhlar, J. Phys. Chem. B **111**, 408 (2007).
[62]D. Martin, A. Weise, and H.-J. Niclas, Angew. Chem., Int. Ed. **6**, 318 (1967).
[63]H. Komber, S. Müllers, F. Lombeck, A. Held, M. Walter, and M. Sommer, Polym. Chem. **5**, 443 (2014).
[64]V. I. Minkin, Chemical Reviews **104**, 2751 (2004).
[65]For $\beta = 2.4$ and $\gamma = 72\,\mathrm{dyn\,cm^{-1}}$ we obtain $\Delta G^*_\mathrm{S} = -97\,\mathrm{kJ\,mol^{-1}}$ instead of $-37\,\mathrm{kJ\,mol^{-1}}$ for Bondi[36] van der Waals radii.
[66]J. F. Kögel, T. Linder, F. G. Schröder, J. Sundermeyer, S. K. Goll, D. Himmel, I. Krossing, K. Kütt, J. Saame, and I. Leito, "Fluoro- and Perfluoralkylsulfonyl-pentafluoroanilides: Synthesis and Characterization of New NH-Acids for Weakly Coordinating Anions and their Gas Phase and Solution Acidities." To be published.
[67]E. Bitzek, P. Koskinen, F. Gähler, M. Moseler, and P. Gumbsch, Phys. Rev. Lett. **97**, 170201 (2006).
[68]1-N-butyl-3-methylimidazolium (BMIm+) is also named as [C4 mim]+ or C4 C1 im+ in the literature.
[69]S. F. L. Mertens, C. Vollmer, A. Held, M. H. Aguirre, M. Walter, C. Janiak, and T. Wandlowski, Angew. Chem., Int. Ed. **50**, 9735 (2011).
[70]A. Held, M. Moseler, and M. Walter, Phys. Rev. B **87**, 045411 (2013).
[71]M. Abareshi, E. K. Goharshadi, and S. M. Zebarjad, J. Mol. Liq. **149**, 66 (2009).
[72]J. Jacquemin, P. Husson, A. A. H. Padua, and V. Majer, Green Chem. **8**, 172 (2006).
[73]J. R. Pliego and J. M. Riveros, J. Phys. Chem. A **105**, 7241 (2001).

[74]D. Himmel, S. K. Goll, I. Leito, and I. Krossing, Chem. Eur. J. **17**, 5808 (2011).

[75]V. Barone, M. Cossi, and J. Tomasi, J. Chem. Phys. **107**, 3210 (1997).

[76]bwGRiD (http://www.bw-grid.de), member of the German D-Grid initiative, funded by the Ministry for Education and Research and the Ministry for Science, Research and Arts Baden-Wuerttemberg.